J|A|C|S
ARTICLES
Published on Web 09/17/2005

Spectroscopic and Electronic Structure Studies of the Trinuclear Cu Cluster Active Site of the Multicopper Oxidase Laccase: Nature of Its Coordination Unsaturation

Liliana Quintanar,[§] Jungjoo Yoon,[§] Constantino P. Aznar,[‡] Amy E. Palmer,[§] K. Kristoffer Andersson,[†] R. David Britt,[‡] and Edward I. Solomon*,[§]

Contribution from the Department of Chemistry, Stanford University, Stanford, California 94305-5080, Department of Chemistry, University of California, Davis, California 95616, and Department of Molecular Biosciences, University of Oslo, N-0316, Norway

Received December 31, 2004; E-mail: edward.solomon@stanford.edu

Abstract: Laccase is a multicopper oxidase that contains four Cu ions, one type 1 (T1), one type 2 (T2), and a coupled binuclear type 3 Cu pair (T3). The T2 and T3 centers form a trinuclear Cu cluster that is the active site for O_2 reduction to H_2O. A combination of spectroscopic and DFT studies on a derivative where the T1 Cu has been replaced by a spectroscopically innocent Hg^{2+} ion has led to a detailed geometric and electronic structure description of the resting trinuclear Cu cluster, complementing crystallographic results. The nature of the T2 Cu ligation has been elucidated; this site is three-coordinate with two histidines and a hydroxide over its functional pH range (stabilized by a large inductive effect, cluster charge, and a hydrogen-bonding network). Both the T2 and T3 Cu centers have open coordination positions oriented toward the center of the cluster. DFT calculations show that the negative protein pocket (four conserved Asp/Glu residues within 12 Å) and the dielectric of the protein play important roles in the electrostatic stability and integrity of the highly charged, coordinatively unsaturated trinuclear cupric cluster. These tune the ligand binding properties of the cluster, leading to its high affinity for fluoride and its coordination unsaturation in aqueous media, which play a key role in its O_2 reactivity.

Introduction

The multicopper oxidases are a family of enzymes that couple the four-electron reduction of O_2 to H_2O with four one-electron oxidations of substrates.[1] The active sites in these proteins include at least four Cu atoms that are classified into three types of sites according to their spectroscopic properties: type 1 (T1) or blue Cu, type 2 (T2) or normal Cu, and type 3 (T3) or coupled binuclear Cu sites. The absorption spectrum of the T1 Cu site is characterized by an intense Cys-S to Cu(II) charge-transfer (CT) band at about 600 nm, while its electron paramagnetic resonance (EPR) spectrum exhibits a narrow parallel hyperfine splitting ($A_{\|} = (40-95) \times 10^{-4}$ cm^{-1}). The T2 or normal Cu site is characterized by the lack of strong absorption features and its EPR spectrum exhibits a normal, large parallel hyperfine splitting ($A_{\|} = (140-200) \times 10^{-4}$ cm^{-1}). The T3 site is composed of two Cu(II) atoms antiferromagnetically coupled through a hydroxide bridge. It is characterized by an intense CT band at about 330 nm (originating from the bridging hydroxide) and the lack of an EPR signal, due to the antiferromagnetic coupling. In *Rhus vernicifera* laccase, the T1 Cu site may be selectively replaced by a spectroscopically silent mercury atom, leaving the T2 and T3 sites intact;[2] this derivative is referred to as T1 mercury-substituted (T1Hg) laccase. Early spectroscopic studies performed on the native form[3,4] of laccase and its T1Hg derivative[5] provided the first evidence that the T2 and T3 sites form a trinuclear Cu cluster. This model was later supported by the crystal structure of ascorbate oxidase (AO),[6] and now all crystallographically characterized multicopper oxidases show similar trinuclear arrangements.[7−12] While the main functional role of the T1 Cu site is to shuttle electrons

§ Stanford University.
‡ University of California, Davis.
† University of Oslo.

(1) Solomon, E. I.; Sundaram, U. M.; Machonkin, T. E. *Chem. Rev.* **1996**, *96*, 2563−2605.
(2) Morie-Bebel, M. M.; Morris, M. C.; Menzie, J. L.; McMillin, D. R. *J. Am. Chem. Soc.* **1984**, *106*, 3677−3678.
(3) Allendorf, M. D.; Spira, D. J.; Solomon, E. I. *Proc. Natl. Acad. Sci. U.S.A.* **1985**, *82*, 3063.
(4) Spira-Solomon, D. J.; Allendorf, M. D.; Solomon, E. I. *J. Am. Chem. Soc.* **1986**, *108*, 5318.
(5) Cole, J. L.; Tan, G. O.; Yang, E. K.; Hodgson, K. O.; Solomon, E. I. *J. Am. Chem. Soc.* **1990**, *112*, 2243−2249.
(6) Messerschmidt, A.; Ladenstein, R.; Huber, R.; Bolognesi, M.; Avigliano, L.; Petruzzelli, R.; Rossi, A.; Finazzi-Agro, A. *J. Mol. Biol.* **1992**, *224*, 179−205.
(7) Zaitseva, I.; Zaitsev, V.; Card, G.; Moshov, K.; Bax, B.; Ralph, A.; Lindley, P. *J. Biol. Inorg. Chem.* **1996**, *1*, 15−23.
(8) Bertrand, T.; Jolivalt, C.; Briozzo, P.; Caminade, E.; Joly, N.; Madzak, C.; Mougin, C. *Biochemistry* **2002**, *41*, 7325−7333.
(9) Piontek, K.; Antorini, M.; Choinowski, T. *J. Biol. Chem.* **2002**, *277*, 37663−37669.
(10) Roberts, S.; Weichsel, A.; Grass, G.; Thakali, K.; Hazzard, J.; Tollin, G.; Rensing, C.; Montfort, W. *Proc. Natl. Acad. Sci. U.S.A.* **2002**, *99*, 2766−2771.
(11) Hakulinen, N.; Kiiskinen, L.; Kruus, K.; Saloheimo, M.; Paananen, A.; Koivula, A.; Rouvinen, J. *Nat. Struct. Biol.* **2002**, *9*, 601−605.
(12) Enguita, F.; Martins, L.; Henriques, A.; Carrondo, M. *J. Biol. Chem.* **2003**, *278*, 19416−19425.

10.1021/ja0421405 CCC: $30.25

from the substrate to the cluster, the trinuclear Cu cluster is the site of oxygen reduction[5] in all multicopper oxidases.

Despite the extensive number of multicopper oxidases that have been structurally and spectroscopically characterized, several functionally relevant questions regarding the chemical nature of the trinuclear Cu cluster remain. One has to do with the nature of the water-derived ligand at the T2 site, its protonation state, and its relation to the pH dependence of the enzyme reactivity. Moreover, the origin of the coordination unsaturation of the T2 and T3 sites is not understood (both have open positions directed inside the cluster), and some controversy exists regarding the nature and identity of the paramagnetic center of the cluster.[13−16] The nature of the exogenous ligand binding to the cluster is another point of controversy. Azide and peroxide binding to the cluster have been studied in detail by spectroscopic methods in solution, and it is clear that these ligands bridge the cluster.[4,17,18] However, the crystal structures of the azide- and peroxide-bound forms show an uncoupling of the T3 Cu (i.e., two Cu^{2+} centers at ~5 Å with no bridge).[1,19,20] Azide and peroxide bind to the cluster with low affinity, while one of the unique features of the trinuclear cluster is its extremely high affinity for fluoride.[4,21] Finally, the crystal structures of the resting trinuclear cluster show open coordination positions at both the T2 and T3 centers, indicating that a water or hydroxide ligand from the accessible solvent does not bind within the cluster even though the T2 Cu^{II} is three-coordinate.

In this study, we have used a combination of spectroscopic techniques (multifrequency and pulsed EPR, absorption, circular dichroism (CD), and magnetic circular dichroism (MCD)) that, in correlation with DFT calculations, provide further insight into the nature of the resting trinuclear cluster; in particular, the assignment of the water-derived ligation of the T2 site, the origin of its high affinity for fluoride, its coordination unsaturation, and the contribution of this unsaturation to reactivity.

Experimental Section

All chemicals were reagent grade and used without further purification. Water was purified to a resistivity of 15−17 MΩ cm^{-1} using a Barnstead Nanopure deionizing system. *Rhus vernicifera* laccase was isolated from acetone powder (Saito and Co., Osaka, Japan) according to published procedures.[22,23] The T1Hg derivative of laccase was prepared using a hollow fiber dialysis unit (Spectrum) as previously described.[2,24,25] Protein concentration was determined using the extinction coefficient of the absorption band at 280 nm (90 000 M^{-1} cm^{-1}). Copper content was determined spectrophotometrically using 2,2′-biquinoline[26] or by atomic absorption spectroscopy. The concentration of paramagnetic copper was determined from spin quantitation of EPR spectra, using a 1.0 mM $CuSO_4 \cdot 5H_2O$ solution with 2 mM HCl and 2 M $NaClO_4$ standard.[27]

Protein samples were buffer-exchanged into 100 mM potassium phosphate buffer (for pH 6.5−8.5), 100 mM MES buffer (for pH 4.7−6.5), or 100 mM CAPS buffer (for pH 8.5−10). For CD and MCD experiments, samples were prepared in deuterated buffers (prepared with 99.99% D_2O). Glassed samples for MCD experiments were prepared by adding 50% (v/v) buffer/glycerol-d_3. Addition of glycerol had no effect on the CD spectrum of the enzymes. Fluoride-bound samples were prepared by incubating the protein with 1−5 equiv of sodium fluoride for 24 h at 4 °C.

X- and Q-band EPR spectra were obtained using a Bruker EMX spectrometer. X-band spectra were obtained using an ER 041 XG microwave bridge and an ER 4102ST cavity. The conditions used for X-band spectra were 9.4 GHz microwave frequency, temperature 77 K, 10 mW microwave power, 20 G modulation amplitude, 100 kHz modulation frequency, 327 ms time constant, and 82 ms conversion time; six scans were averaged. Q-band spectra were obtained using an ER 051 QR microwave bridge, an ER 5106QT resonator, and an Oxford continuous-flow CF935 cryostat. Conditions for Q-band spectra were 34 GHz microwave frequency, temperature 70 K, 0.37 mW microwave power, 10 G modulation amplitude, 100 kHz modulation frequency, 327 ms time constant, and 163 ms conversion time; six scans were averaged. High-frequency EPR measurements were performed using a spectrometer built in the Grenoble High Magnetic Field Laboratoty (GHMFL), with a Gunn diode (Radiometer Physics, Germany), its multipliers (for 95−285 GHz), and a superconducting magnet (Cryogenics Consultant, UK) equipped with a bipolar power supply (Oxford Instruments, UK). The magnetic field homogeneity was about 50 ppm within a 10 mm diameter sphere. The light transmitted through the sample was detected with an InSb bolometer (QMC Instruments). Samples were prepared in small cylindrical Teflon holders containing 250−300 μL of 2 mM protein. Conditions for high-field spectra were 285 GHz microwave frequency, temperature 15 K, 1 mT modulation amplitude, 10 kHz modulation frequency, and 300 ms time constant. All EPR spectra were baseline-corrected and simulated using XSophe (Bruker).

Pulsed EPR and electron nuclear double-resonance (ENDOR) experiments were performed on a laboratory-built spectrometer described previously.[28] For three-pulsed electron spin−echo envelope modulation (ESEEM), the echo was monitored by incrementing T in the pulse sequence $\pi/2-\tau-\pi/2-T-\pi/2-\tau-$echo. A cosine Fourier backfill procedure as described by Mims[29] was used to reconstruct instrumental dead time in order to generate the frequency-domain ESEEM spectra. In electron spin−echo ENDOR (ESE-ENDOR) experiments, two methods were used: ^{2}H Mims ENDOR was performed following the pulse scheme $\pi/2-\tau-\pi/2-T-\pi/2-$echo,[30] and Davies ENDOR was performed to obtain ^{1}H and ^{14}N ENDOR spectra using the pulse-echo sequence $\pi-T-\pi/2-\tau-\pi-\tau-$echo.[31] In both pulsed ENDOR techniques, T is the mixing period during which the radio frequency pulse of variable frequency is applied to drive the nuclear transition. All experiments were performed at an X-band frequency of 10.88 GHz and temperature of 10 K.

Room-temperature UV−visible absorption spectra were recorded using a Hewlett-Packard HP8452A or an Agilent 8453 diode array spectrophotometer. Room-temperature CD and low-temperature (5 K) MCD spectra in the UV−visible region were collected with a Jasco J-810-150S spectropolarimeter operating with an S-20 photomultiplier

(13) Morie-Bebel, M. M.; McMillin, D. R.; Antholine, W. E. *Biochem. J.* **1986**, *235*, 415−420.
(14) Fraterrigo, T. L.; Miller, C.; Reinhammar, B.; McMillin, D. R. *J. Biol. Inorg. Chem.* **1999**, *4*, 183−187.
(15) Li, J.; McMillin, D. R.; Antholine, W. E. *J. Am. Chem. Soc.* **1992**, *114*, 725−727.
(16) Bonomo, R. P.; Castronovo, B. M. G.; Santoro, A. M. *Dalton Trans.* **2004**, *1*, 104−112.
(17) Cole, J. L.; Clark, P. A.; Solomon, E. I. *J. Am. Chem. Soc.* **1990**, *112*, 9534−9548.
(18) Sundaram, U. M.; Zhang, H. H.; Hedman, B.; Hodgson, K. O.; Solomon, E. I. *J. Am. Chem. Soc.* **1997**, *119*, 12525−12540.
(19) Messerschmidt, A.; Luecke, H.; Huber, R. *J. Mol. Biol.* **1993**, *230*, 997−1014.
(20) Zaitsev, V. N.; Zaitseva, I.; Papiz, M.; Lindley, P. F. *J. Biol. Inorg. Chem.* **1999**, *4*, 579−587.
(21) Brändén, R.; Malmstrom, B. G.; Vänngard, T. *Eur. J. Biochem.* **1973**, *36*, 195−200.
(22) Reinhammar, B. *Biochim. Biophys. Acta* **1970**, *205*, 35−47.
(23) Reinhammar, B. R. M. *Biochim. Biophys. Acta* **1972**, *275*, 245−259.
(24) Morie-Bebel, M. M.; Menzie, J. L.; McMillin, D. R. In *Conference on Copper Coordination Chemistry*; Karlin, K. D., Zubieta, J., Eds.; Adenine Press: Guilderland, NY, 1984; Vol. 1, pp 89 ff.
(25) Severns, J. C.; McMillin, D. R. *Biochemistry* **1990**, *29*, 8592−8597.
(26) Felsenfeld, G. *Arch. Biochem. Biophys.* **1960**, *87*, 247−251.
(27) Carithers, R. P.; Palmer, G. *J. Biol. Chem.* **1981**, *256*, 7967−7976.
(28) Sturgeon, B. E.; Britt, R. D. *Rev. Sci. Instrum.* **1992**, *63*, 2186−2192.
(29) Mims, W. B. *J. Magn. Reson.* **1984**, *59*, 291−306.
(30) Mims, W. B. *Proc. R. Soc. London* **1965**, *283*, 452.
(31) Davies, E. R. *Phys. Lett.* **1974**, *47A*, 1−2.

tube and an Oxford SM4000-8T magnet. CD and MCD spectra in the near-IR region were obtained with a Jasco J-200-D spectropolarimeter, using a liquid-nitrogen-cooled InSb detector and an Oxford SM4000-7T magnet. CD samples were run in a 0.5 cm quartz cuvette. MCD samples were run in cells fitted with quartz disks and a 3 mm rubber spacer. All MCD spectra presented are the subtracted average of the +7 T and −7 T scans (at least four scans each), [7 − (−7)]/2 T, to eliminate glass-induced baseline shifts and to increase signal-to-noise ratios. Gaussian fitting of the absorption, CD, and MCD spectra was performed using PeakFit 4.0 (Jandel).

Spin-unrestricted DFT calculations were performed on a PC cluster using Gaussian 98,[32] and the resulting molecular orbitals were visualized using Molden[33] and analyzed using AOMix.[34,35] Broken-symmetry wave functions[36] were obtained to account for the multideterminantal character in the antiferromagnetically coupled ground states.[37] All geometry optimizations were performed at the uB3lyp/Lanl2dz level.[38−42] The geometry of the trinuclear Cu^{II} site was adapted from the crystal structure of AO[6] in which the side chains to the protein backbone were truncated and replaced by hydrogen atoms. The positions of these hydrogens and those involved in hydrogen bonds were fixed in the optimizations to reflect contributions from the protein environment. The resulting optimized structures were then used for single-point calculations with spectroscopically calibrated B38HFP86 hybrid functionals (38% Hartree−Fock exchange added to the BP86 functional)[43] using the triple-ζ-quality all-electron contracted-Gaussian basis sets of Schäfer et al.[44] with additional polarization functions[43] on the coppers and the double-ζ basis sets with polarization 6-31G(d) on all the other elements (VTZ*+6-31G*). Solution structures were calculated by Tomasi's reaction field method using the polarized continuum model (PCM) as implemented in Gaussian 98. The dielectric constant was set equal to 5.0 to simulate the dielectric medium of the protein interior. Models with NH_3, rather than the imidazolyl ligands, have been calculated to monitor the effects of the dielectric medium, as most of the models with the imidazolyl ligands and three coppers were too large for PCM calculations.

Results and Analysis

1. Electronic Structure of the Resting Trinuclear Cluster. 1.1. Spectroscopic Characterization of the Resting T2 Site. 1.1.1. Multifrequency EPR. The EPR spectrum of the T2 site in T1Hg laccase has been collected at different microwave frequencies. The X-band EPR spectrum of T1Hg laccase at 77 K (Figure 1A) shows the typical features of the T2 site as previously reported,[1] with $g_{\|} > g_{\perp} > 2.00$ and a large parallel hyperfine splitting, associated with a $d_{x^2-y^2}$ ground state. In the Q-band EPR spectrum at 34 GHz (Figure 1B), the parallel region is clearly resolved and all four transitions derived from the Cu ($I = {}^3/_2$) hyperfine splitting can be directly observed. The structure observed in the perpendicular region of both the X- and Q-band spectra is due to nitrogen hyperfine splitting from the histidine ligands. At 285 GHz (Figure 1C), the rhombicity at the perpendicular region of the EPR spectrum is resolved and the features associated with g_x and g_y were directly measured. The simultaneous fit of these multifrequency EPR spectra yields the parameters listed in Table 1, and the simulated spectra are shown in dotted lines in Figure 1.

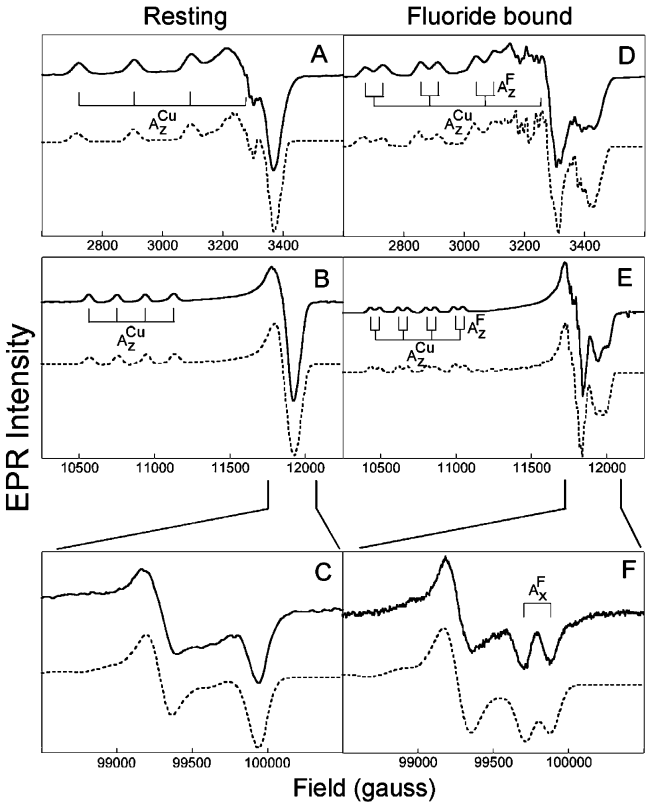

Figure 1. Multifrequency EPR spectra. X-band (A), Q-band (B), and 285 GHz (C) spectra of T1Hg laccase in the resting form. X-band (D), Q-band (E), and 285 GHz (F) spectra of T1Hg laccase with one fluoride bound. The 285 GHz spectra show the perpendicular region only. Experimental data are shown in solid lines, and the simulated spectra obtained with the parameters listed in Table 1 are shown in dotted lines. Spectra were taken under the conditions specified in the Experimental Section.

Table 1. EPR Parameters of the T2 Site in the Resting and Fluoride-Bound Forms of T1Hg Laccase[a]

	resting	fluoride-bound		resting	fluoride-bound
g_x	2.041	2.047	A_y^N	16	16
g_y	2.054	2.058	A_z^N	14	14
g_z	2.241	2.263	A_x^F		160
A_x	22	25	A_y^F		63
A_y	18	22	A_z^F		63
A_z	193	192	A^N (ENDOR)	14.6	13.8
A_x^N	15	15			

[a] The hyperfine coupling constants are reported in $X \times 10^{-4}$ cm^{-1}, and the error associated with them is ±2.

From ligand field theory,[45] the difference between the g values and 2.00 are inversely proportional to the ligand field transition energies, and directly proportional to the Stevens orbital reduction factor (which is an indication of the covalency at the half-occupied HOMO). The rhombicity of the T2 site ($g_y - g_x = 0.013$) is very small (Figure 1C) and originates from the energy splitting between the d_{xz} and $d_{yz} \rightarrow d_{x^2-y^2}$ ligand field transitions, as observed by MCD (section 1.1.5).

(32) Frisch, M. J.; et al. *Gaussian 98*, revision A.11.3; Gaussian, Inc.: Pittsburgh, PA, 1998.
(33) Schaftenaar, G.; Noordik, J. H. J. *Comput. Aided Mol. Des.* **2000**, *14*, 123−124.
(34) Gorelsky, S. I. *AOMix program*, revision 5.83; http://www.sg-chem.net/.
(35) Gorelsky, S. I.; Lever, A. B. P. *J. Organomet. Chem.* **2001**, *635*, 187−196.
(36) Noodleman, L. *J. Chem. Phys.* **1981**, *74*, 5737−5743.
(37) Tuczek, F.; Solomon, E. I. *J. Am. Chem. Soc.* **1994**, *116*, 6916−6924.
(38) Becke, A. D. *J. Chem. Phys.* **1993**, *98*, 5648−5652.
(39) Dunning, T. H. J.; Hay, P. J. In *Modern Theoretical Chemistry*; Schaefer, H. F., III, Ed.; Plenum: New York, 1976; Vol. 3, p 1.
(40) Hay, P. J.; Wadt, W. R. *J. Chem. Phys.* **1985**, *82*, 270−283.
(41) Hay, P. J.; Wadt, W. R. *J. Chem. Phys.* **1985**, *82*, 299−310.
(42) Wadt, W. R.; Hay, P. J. *J. Chem. Phys.* **1985**, *82*, 284−298.
(43) Szilagyi, R. K.; Metz, M.; Solomon, E. I. *J. Phys. Chem. A* **2002**, *106*, 2994−3007.
(44) Schäfer, A.; Horn, H.; Ahlrichs, R. *J. Chem. Phys.* **1992**, *97*, 2571−2577.
(45) McGarvey, B. R. In *Transition Metal Chemistry*; Carlin, B. L., Ed.; Marcel Dekker: New York, 1966; Vol. 3, pp 89−201.

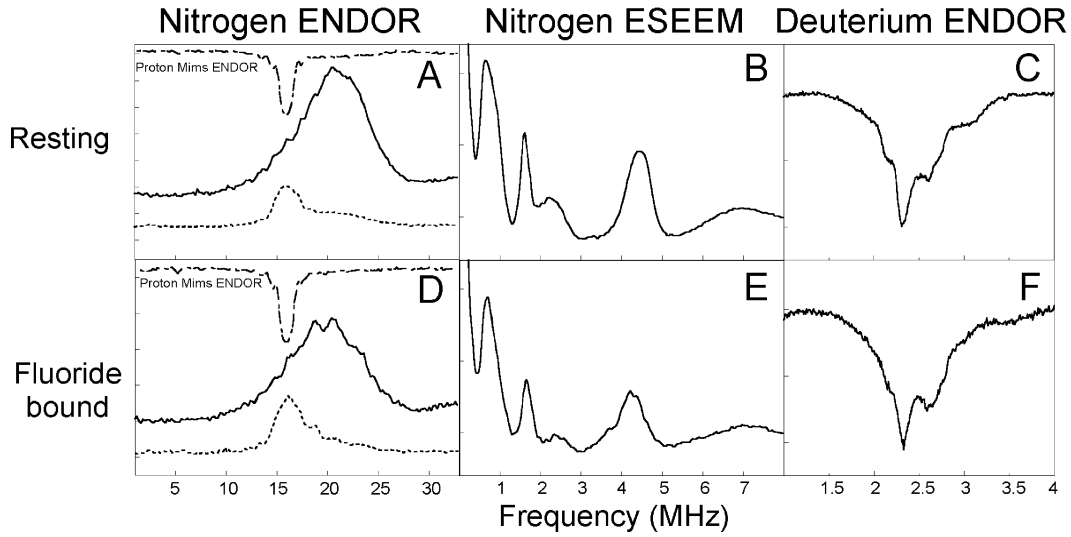

Figure 2. Pulsed EPR spectra. Davies ENDOR of T1Hg laccase resting (A) and fluoride-bound (D), at microwave pulses: $\pi = 60$ ns and $\pi/2 = 30$ ns (—), and $\pi = 400$ ns and $\pi/2 = 200$ ns (- - -); for both, $\tau = 450$ ns, $T = 40$ ms (time between first and second pulse), and 30 μs radio frequency pulse; proton Mims ENDOR is shown for comparison (— - —). Nitrogen ESEEM spectra of T1Hg laccase resting (B) and fluoride-bound (E) at $\tau = 187$ ns. Deuterium Mims ENDOR on T1Hg laccase resting (C) and fluoride-bound (F); $\tau = 476$ ns, microwave pulse $\pi/2 = 15$ ns, and 40 μs radio frequency pulse. All spectra were collected at 10 K, microwave frequency 10.876 GHz, and field 3760 G.

An estimate for the % Cu character of the ground-state wave function can be made from an analysis of the spin Hamiltonian parameters in Table 1. From ligand field theory, the metal hyperfine couplings are given by

$$A_x = P_d\left[-\kappa + \frac{2\alpha^2(a^2-b^2)}{7} + \frac{\alpha^2 4ab\sqrt{3}}{7} + (g_x - 2.0023) - \frac{(3a-\sqrt{3}b)(g_y-2.0023)}{14(a+\sqrt{3}b)} - \frac{b(g_z-2.0023)}{7a}\right] \quad (1a)$$

$$A_y = P_d\left[-\kappa + \frac{2\alpha^2(a^2-b^2)}{7} - \frac{\alpha^2 4ab\sqrt{3}}{7} + (g_y - 2.0023) - \frac{(3a+\sqrt{3}b)(g_x-2.0023)}{14(a-\sqrt{3}b)} - \frac{b(g_z-2.0023)}{7a}\right] \quad (1b)$$

$$A_z = P_d\left[-\kappa - \frac{4\alpha^2(a^2-b^2)}{7} + \frac{(3a-\sqrt{3}b)(g_y-2.0023)}{14(a+\sqrt{3}b)} + \frac{(3a+\sqrt{3}b)(g_x-2.0023)}{14(a-\sqrt{3}b)} + (g_z - 2.0023)\right] \quad (1c)$$

where P_d is 400×10^{-4} cm^{-1} for Cu(II), κ is the Fermi contact contribution due to spin polarization, α^2 is the percent metal character in the ground-state wave function (reduced from 1.0 due to covalent electron delocalization onto the ligand orbitals), and a and b are the $d_{x^2-y^2}$ and d_{z^2} contributions to the ground-state wave function, respectively. No significant amount of d_{z^2} mixing into the ground state is obtained by DFT calculations (section 1.3). Using the experimental g values, the A values can be best fit with a Fermi contact κ of 0.30 (reduced from the copper atom value of 0.43[46] due to covalency) and α^2 of 0.72, indicating that the Cu character of the ground state is ~70%.

1.1.2. Nitrogen ENDOR. The Davies ENDOR spectrum of T1Hg laccase at pH 7.5 and 10 K (Figure 2A) shows resonances from both protons and nitrogens that are strongly coupled with the paramagnetic T2 Cu center. As the length of the microwave pulse is decreased, the contribution of weakly coupled protons is suppressed[47] and the contributions from ligands with sufficiently high hyperfine coupling constants are accentuated. With the long $\pi = 400$ ns and $\pi/2 = 200$ ns pulses (dotted line in Figure 2A), the resonances from protons dominate the spectrum at ~16 MHz, the Larmor frequency for ^{1}H. The Mims ENDOR spectrum, where a strong signal from weakly coupled protons (e.g., ambient waters) appears at the same frequency, is shown for comparison in Figure 2A (dashed line). In contrast, with the short $\pi = 60$ ns and $\pi/2 = 30$ ns pulses (solid line in Figure 2A), the signals from the strongly coupled nitrogens are enhanced. This signal originates from the coordinating nitrogens of the histidine ligands and yields an $A^N/2$ of 21.9 MHz. The signal is broad and its components could not be resolved by scanning at different fields, indicating that the coordinating nitrogens are approximately equivalent and their anisotropy is small. The equivalency of the histidine ligands is consistent with the nitrogen ESEEM results (section 1.1.3). Also, the small anisotropy observed is consistent with ENDOR studies on Cu—imidazole complexes[48] and on blue copper proteins,[49,50] which have found that the nitrogen coupling constants from the histidine ligands show at most 10% anisotropy. The experimental $A^N = 43.8$ MHz (14.6×10^{-4} cm^{-1}) is obtained at the

(46) Gewirth, A. A.; Cohen, S. L.; Schugar, H. J.; Solomon, E. I. *Inorg. Chem.* **1987**, *26*, 1133—1146.

(47) Doan, P. E.; Fan, C.; Davoust, C. E.; Hoffman, B. M. *J. Magn. Reson.* **1991**, *95*, 196—200.

(48) van Camp, H. L.; Sands, R. H.; Fee, J. A. *J. Chem. Phys.* **1981**, *75*, 2098—2107.

(49) Roberts, J. E.; Cline, J. F.; Lum, V.; Freeman, H.; Gray, H. B.; Peisach, J.; Reinhammar, B.; Hoffman, B. M. *J. Am. Chem. Soc.* **1984**, *106*, 5324—5330.

(50) Werst, M. M.; Davoust, C. E.; Hoffman, B. M. *J. Am. Chem. Soc.* **1991**, *113*, 1533—1538.

perpendicular region of the EPR spectrum, which corresponds to a distribution from

$$A_{||}^{N} = \beta^2[n^2A_{iso} + (1 - n^2)A_{aniso}] \quad \text{to}$$
$$A_{\perp}^{N} = \beta^2[n^2A_{iso} - {}^1/_2(1 - n^2)A_{aniso}] \quad (2)$$

where β^2 is the electron spin density at the coupled nitrogen, n^2 is the s character of the nitrogen hybrid orbital ($1 - n^2$ is 2p character), and A_{iso} and A_{aniso} for ^{14}N are 600×10^{-4} and 30×10^{-4} cm^{-1}, respectively.[51,52] Considering sp^2 hybridization for the histidine nitrogen donor orbital (i.e., $n^2 = 1/3$), one can estimate that the spin density at each of the coupled nitrogens is 7−8%. Taking into account our nitrogen ESEEM results (section 1.1.3), two histidine ligands would contribute a total of ∼15% of the spin density to the ground state of the T2 site. It should be noted that this analysis estimates 5% anisotropy, consistent with the above-mentioned studies on blue copper proteins.

1.1.3. Nitrogen ESEEM. The frequency spectrum obtained from the Fourier transform of the three-pulse ESEEM spectrum of T1Hg laccase at 10 K is shown in Figure 2B. The spectrum was taken at $\tau = 187$ ns, suppressing proton contributions and allowing the isolation of the signals from the remote nitrogens of the coordinating histidine ligands. The directly coordinated nitrogens do not contribute to the ESEEM spectrum.[53] The intense lines observed below 2 MHz correspond to the zero-field nuclear quadrupole frequencies, while the broad feature at 4 MHz corresponds to the double-quantum peak, which is dependent on the nitrogen hyperfine couplings. A combination peak is observed at around 2.5 MHz, indicating the presence of more than one coordinated imidazole in approximately equivalent positions.[54] Simulations of the spectrum in Figure 2B were performed using the Hamiltonian operator:

$$H = SA_N \cdot I - g_N\beta_N H \cdot I + \frac{e^2qQ}{4}[3I_z^2 - 2 + \eta(I_x^2 - I_y^2)] \quad (3)$$

where $e^2qQ/4$ is the quadrupole coupling constant and η is the asymmetry parameter. The parameters used in the simulations were $A_{iso} = 1.75$ MHz, $A_{dip} = 0.2$ MHz, $e^2Qq = 1.55$ MHz, and $\eta = 0.85$. The ESEEM data can be best fit with two histidine ligands (Figure S1, Supporting Information), consistent with previous pulsed EPR studies performed in T1Hg laccase.[54] On the basis of an S-band EPR study on T1Hg laccase, it has previously been proposed that the T2 site possesses three histidine ligands;[13] however, a comparison of simulations with two and three coordinated histidines with our data (Figure S1, Supporting Information) shows that the depth of the modulation in the time domain spectrum is best fit with two histidine ligands. Therefore, our and previous[54] pulsed EPR studies argue for the T2 site having two histidine ligands, consistent with crystallographic results done at 277 K[6] and cryo temperatures.[7−12]

1.1.4. Deuterium ENDOR. The width of the Mims deuterium ENDOR spectrum of T1Hg laccase in Figure 2C denotes the presence of strongly coupled deuteron(s). This is confirmed by the ^{1}H two-pulse ESEEM spectrum (Figure S2, Supporting Information), where a significant peak shift is observed from the negative sum combination peak ($2\nu_H$). However, the number of strongly coupled protons and their hyperfine couplings could not be accurately determined.[55] Thus, to elucidate the nature of the water-derived ligand at the T2 site, pH studies on the spectroscopic features of the T2 site were undertaken (section 1.1.6).

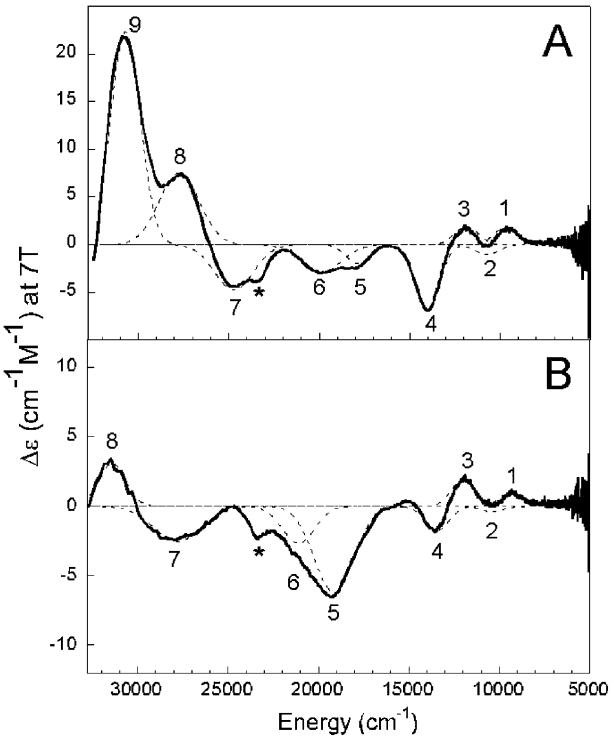

Figure 3. MCD spectra of T1Hg laccase resting (A) and fluoride-bound (B) at pD 7.5 and 5 K. Resolved component Gaussian bands are shown in dotted lines, and their parameters are listed in Table 2. A small amount of heme impurity (∗) was present in the samples.

The analysis of the multifrequency and pulsed EPR data has yielded the composition of the ground-state wave function of the T2 site in resting T1Hg laccase, which serves as a reference for DFT calculations (section 1.3). The oxygen character can be estimated from previous EPR studies on fungal laccase in ^{17}O water,[56] which determined a superhyperfine coupling constant of 12×10^{-4} cm^{-1} at the parallel region of the T2 signal (the perpendicular region was obscured by the T1 site signal). Considering that this coupling represents a lower limit in the range of orientation-dependent couplings, and assuming an oxygen donor orbital with purely p character, a spin density of at least 13% at the oxygen is estimated.

1.1.5. MCD. As previously reported,[17,18] only the paramagnetic T2 site contributes to the MCD spectrum of T1Hg laccase at 5 K (Figure 3A). The spectrum can be resolved into nine Gaussian bands, as listed in Table 2. Bands 1−4 are assigned as ligand field transitions; the presence of negative band 2 is justified by the comparison to the spectrum at low pH, which clearly shows a negative band at this energy (section 1.1.6). The assignment in Table 2 differs from the previous assign-

(51) Goodman, B. A.; Raynor, J. B. *Adv. Inorg. Chem. Radiochem.* **1970**, *13*, 135−362.
(52) Weil, J. A.; Bolton, J. R.; Wertz, J. E. *Electron Paramagnetic Resonance: Elementary Theory and Practical Applications*; Wiley-Interscience: New York, 1994.
(53) Mims, W. B.; Peisach, J. *J. Chem. Phys.* **1978**, *69*, 4921−4930.
(54) Lu, J.; Bender, C. J.; McCracken, J.; Peisach, J.; Severns, J. C.; McMillin, D. R. *Biochemistry* **1992**, *31*, 6265−6272.
(55) To fully describe the number of protons and their hyperfine coupling parameters, data acquisition at *g* parallel with smaller τ is required.
(56) Deinum, J. S.; Vanngard, T. *FEBS Lett.* **1975**, *58*, 62−65.

Table 2. T2 Site MCD Transition Energies (cm^{-1})

band assignment	T1Hg resting	T1Hg fluoride adduct
1 *xy*	(+) 9 700	(+) 9 300
2 z^2	(−) 10 700	(−) 10 400
3 *xz*	(+) 11 800	(+) 12 000
4 *yz*	(−) 14 000	(−) 13 400
5 His π_1 CT	(−) 17 900	(−) 19 100
6 OH π CT	(−) 19 900	(−) 21 100
7 His π_1 CT	(−) 24 700	(−) 27 800
8 His π_2 CT	(+) 27 700	(+) 31 400
9 His π_2 CT	(+) 30 700	ND

ment[18] in the relative position of the $d_{z^2} \rightarrow d_{x^2-y^2}$ transition, which is derived from TD-DFT calculations (Table S1, Supporting Information).

Bands 5−9 are assigned as ligand-to-metal charge-transfer (LMCT) bands. Studies of Cu−imidazole complexes have shown that each imidazole ligand generates two π (π_1 and π_2) $\rightarrow Cu^{2+}$ transitions and one $\sigma \rightarrow Cu^{2+}$ CT transition;[57,58] the latter is at high energy and cannot be accessed in the spectra of Cu proteins. The $\pi_1 \rightarrow Cu^{2+}$ CT transitions originate from a mostly carbon-based orbital and appear at lower energy (27 000−30 000 cm^{-1}) than the $\pi_2 \rightarrow Cu^{2+}$ transitions (32 500−38 000 cm^{-1}), which originate from a mostly nitrogen-based orbital. Considering that these studies pertain to four-coordinate sites, and that CT transitions shift to lower energy (by ∼6000 cm^{-1}) with a decrease in coordination number (due to decreased destabilization of the d-manifold),[59] low-energy N(His) $\pi \rightarrow Cu^{2+}$ CT transitions can be expected for the three-coordinate T2 site in T1Hg laccase. Crystallography and our ESEEM studies indicate that the T2 site possesses two histidine ligands; therefore, a total of four His $\pi \rightarrow Cu^{2+}$ CT bands would be observed in the MCD spectrum of T1Hg laccase. According to their energies, four of the five bands 5−9 can be reasonably assigned to these transitions; the fifth should originate from the hydroxide ligand (vide infra).

A hydroxide ligand at the T2 Cu would yield a high-intensity σ (OH) $\rightarrow Cu^{2+}$ CT transition, which would be at too high an energy to access.[60,61] A π (OH) $\rightarrow Cu^{2+}$ CT transition is expected at lower energy and with an intensity comparable to that of the LF transitions, as predicted by TD-DFT calculations (Table S1, Supporting Information). Since band 6 is the only CT band that shows intensity changes with pH variation (section 1.1.6, Figure 4A), we assign it to the π (OH) $\rightarrow Cu^{2+}$ CT transition. In summary, the MCD spectrum of the T2 site in T1Hg laccase exhibits very low-energy LMCT bands, compared to four-coordinate Cu model complexes, consistent with its three-coordinate structure.

(57) Bernanducci, E. E.; Schwindinger, W. F.; Hughey, J. L.; Krogh-Jespersen, K.; Schugar, H. J. *J. Am. Chem. Soc.* **1981**, *103*, 1686−1691.
(58) Fawcett, T. G.; Bernanducci, E. E.; Krogh-Jespersen, K.; Schugar, H. J. *J. Am. Chem. Soc.* **1980**, *102*, 2598−2604.
(59) Gamelin, D. R.; Randall, D. W.; Hay, M. T.; Houser, R. P.; Mulder, T. C.; Canters, G. W.; de Vries, S.; Tolman, W. B.; Lu, Y.; Solomon, E. I. *J. Am. Chem. Soc.* **1998**, *120*, 5246−5263.
(60) None of the CT bands observed in Figure 3A can be assigned as the σ (OH) CT transition; the T2 site does not contribute significant absorption intensity in this region, as indicated by a spectral comparison of T1Hg laccase with the T2-depleted (T2D) form of laccase (Figure S3, Supporting Information). The σ (OH) $\rightarrow Cu^{2+}$ CT transition must be at higher energy than the 300 nm protein cutoff. This is consistent with spectroscopic studies of a mononuclear tris(pyrazolyl)borate hydroxocopper(II) complex, where no OH $\rightarrow Cu^{2+}$ CT transition was observed in the 8000−30 000 cm^{-1} region.[61]
(61) Chen, P.; Fujisawa, K.; Solomon, E. I. *J. Am. Chem. Soc.* **2000**, *122*, 10177−10193.

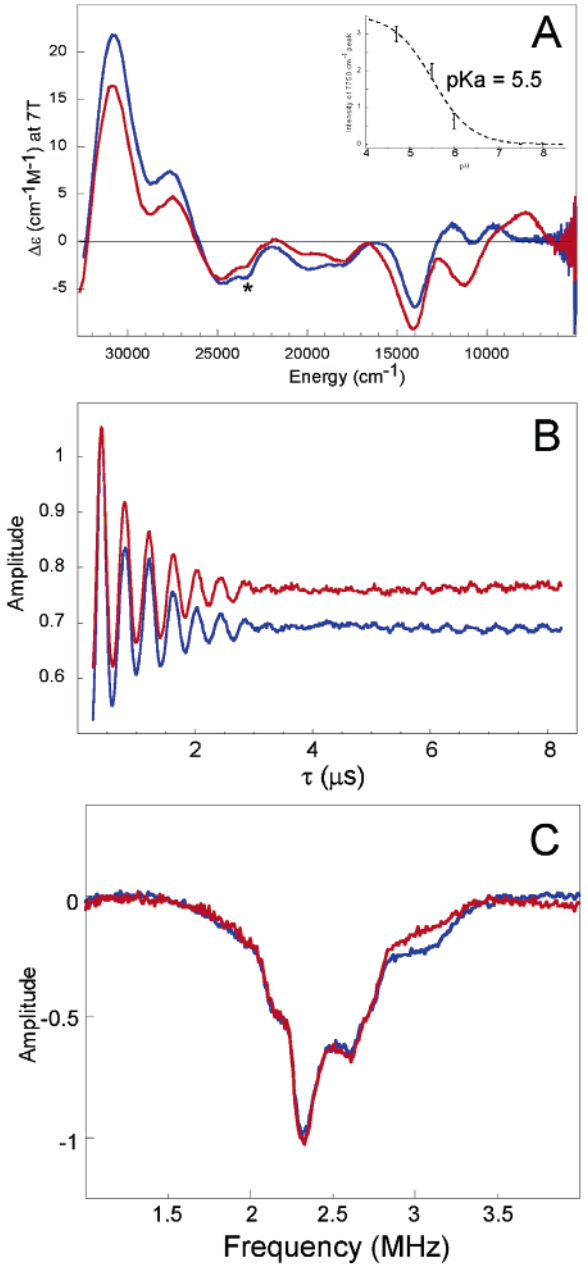

Figure 4. (A) MCD spectra of T1Hg laccase resting at pD 7.5 (blue) and pD 4.7 (red), at 5 K. Inset: pH dependence of the intensity at the 7700 cm^{-1} peak (circles) and fit to the data (dotted lines), indicating a pK_a of 5.5. A small amount of heme impurity (∗) was present in the samples. Ratioed (pD/pH) ESEEM (B) and deuterium ENDOR (C) spectra of T1Hg laccase resting at pD 7.5 (blue) and pD 4.7 (red), at 10 K.

1.1.6. pH Perturbation of the T2 Site. The spectroscopic features of the T2 site were investigated as a function of pH to elucidate the nature of its water-derived ligand. No changes were observed in the MCD spectrum of T1Hg laccase in the range from 9.6 to 7.5; however, significant changes of the ligand field transitions of the T2 site were observed at lower pH. Figure 4A shows the comparison of the MCD spectra taken at pD 7.5 (blue) and pD 4.7 (red). At low pH, a positive band at ∼7800 cm^{-1} grows in; a plot of the intensity of this band as a function of pD is shown in Figure 4A (inset), showing a pK_a of 5.5 ± 0.8 associated with this change.[62] Gaussian analysis of the spectrum at low pH shows that the main effects on the ligand field transitions are the redistribution of intensities and a large

shift of the $d_{xy} \rightarrow d_{x^2-y^2}$ transition (band 1) to lower energy. No significant change is observed in the energies and intensities of the CT bands, indicating that the coordinated residues are not perturbed and that there is no change in the coordination number of the site.

A series of continuous-wave (cw) and pulsed EPR experiments were performed at high and low pH. The multifrequency EPR spectra of T1Hg laccase do not change in the pH range of 4.7−7.5 (Figure S4, Supporting Information). Similarly, the Davies ENDOR and nitrogen ESEEM spectra show no change in this pH range (Figure S5, Supporting Information), indicating that the coordinated histidines are not affected by the pH change. One possibility is that the pH effect is related to a protonation event at the ligand of the T2 site (i.e., a hydroxide/water equilibrium); however, the deuterium ENDOR spectra at pD 7.5 and 4.7 show no differences (Figure 4C), indicating that the strongly coupled proton(s) are not altered in this pH range. Moreover, the modulation depth in the deuterium ESEEM spectra of T1Hg laccase *decreases* at pD 4.7 (Figure 4B), opposite to the behavior expected for the protonation of the hydroxide ligand at low pD (the modulation depth of deuterium ESEEM increases with the number of strongly coupled ^{2}H). Finally, DFT calculations predict large changes in the composition of the ground-state wave function of the T2 site upon protonation of the hydroxide ligand (Table S2, Supporting Information), which would be evident as larger shifts in the *g* values and hyperfine couplings in the cw EPR spectra. However, the EPR spin Hamiltonian parameters do not change over the pH range studied (Figure S4, Supporting Information), indicating that the pH effect is *not* due to a water/hydroxide equilibrium at the T2 center.

The pH range examined limits the pK_a value for the T2 Cu-bound water/hydroxide to be either $\geq$10.3 or $\leq$4. The pK_a of Cu^{2+}-bound water in $Cu(OH_2)_6^{2+}$ and other Cu^{2+} model complexes is about 7.[63−65] Considering that the inductive effect would be much larger for a three-coordinate T2 Cu^{2+} site in a highly positively charged cluster, resulting in a p$K_a \ll 7$, we assign the water-derived ligand at the T2 site as a hydroxide that does not undergo protonation within the pH range studied.

Multifrequency EPR, ENDOR, and ESEEM data indicate that the pH effect observed by MCD is not due to the T2 Cu-bound ligands. To elucidate the origin of this pH effect, the spectroscopic features of the T3 site were also analyzed as a function of pH. Absorption and CD spectra of T1Hg laccase at pD 7.5 and pD 4.7 are identical (Figure S6), indicating that the T3 site is not perturbed over this pH range. Therefore, the pH effect observed by MCD must be due to a protonation event outside the trinuclear cluster, possibly an amino acid residue in the vicinity of the T2 site. Given the pK_a associated with the effect (5.5 ± 0.8), the species involved is likely a carboxylic residue. From the crystal structure of AO,[6] Asp73 (Asp72 in *Rhus vernicifera* laccase)[66] is the closest carboxylic residue and is hydrogen-bonded to a water molecule, which in turn is hydrogen-bonded to the T2 hydroxide ligand. It should be noted that this hydrogen bond arrangement is conserved in the crystal structure of several multicopper oxidases.[9,10,12] Thus, the protonation of Asp73 could perturb the orientation of the hydroxide ligand at the T2 site. Since the π interaction of the OH ligand with the d_{xz} and d_{xy} orbitals is dependent on the orientation of the O−H bond (as indicated by the DFT-derived orbital descriptions in section 1.3), this would also perturb the MCD LF features. To probe this model, more detailed pulsed EPR experiments are underway.

In summary, the spectroscopic characterization of the T2 site in T1Hg laccase and its pH perturbation is consistent with having a three-coordinate site, with two histidines and one hydroxide ligand; a nearby Asp residue appears to have a hydrogen bond connectivity with the T2 hydroxide ligand which affects the relative orientation of the O−H bond.

1.2. Spectroscopic Characterization of the Resting T3 Site. The absorption and CD spectra of resting T1Hg laccase are shown in panels A and C of Figure 5, respectively. The T3 site is the primary contributor to these spectra. As previously reported, the absorption spectrum of T1HgLc shows an intense ($\epsilon \approx 4.2$ mM^{-1} cm^{-1}) transition at ~30 300 cm^{-1}, which has been assigned as a μ-OH $\rightarrow$ Cu^{2+} CT transition.[17,18] Simultaneous Gaussian analysis of the absorption and CD spectra requires the presence of nine bands with the energies listed in Table 3, and shown in Figure 5A,C (dotted lines). On the basis of their high Kuhn anisotropy factors (ratio of CD to absorption intensity, $\Delta\epsilon/\epsilon$, Table 3), bands 1−6 are assigned as LF transitions. The fact that more than four ligand field transitions exist indicates that the two T3 Cu ions are inequivalent. Bands 7−9 have low Kuhn anisotropy factors and are assigned as ligand-to-metal CT transitions. The CD data show that the 330 nm absorption band is actually composed of two bands (bands 8 and 9), consistent with μ-OH CT transitions to the two T3 coppers. Considering that $\pi_1 \rightarrow Cu^{2+}$ CT transitions occur in the range of 27 000−30 000 cm^{-1} in four-coordinate tetragonal imidazole Cu model complexes, and would shift to lower energy as the geometry becomes pseudo-tetrahedral,[57,58,67] band 7 is assigned as a resolvable T3 His $\pi_1 \rightarrow Cu^{2+}$ CT transition.

1.3. DFT Calculations on the Resting Trinuclear Cluster. The geometries of the T2 and T3 sites were optimized separately using the unrestricted B3LYP hybrid functional with LanL2Dz basis set. These two sites were combined and re-optimized to obtain the structure of the trinuclear cluster in the resting oxidized state (T2T3). The T2 and T3 geometries in the resulting T2T3 structure are very similar to those obtained in the separate T2 and T3 optimizations (Table 4). T2+HB and T2T3+HB refer to models with two additional H_2O molecules, mimicking the hydrogen-bonding environment in the vicinity of the T2 site. Overall, reasonable agreement with the crystallography is obtained for all models considered. In particular, the "T"-shape of the T2 Cu and the distorted trigonal bipyramidal shape of the T3 Cu's are retained in these optimizations. Any discrepancy from the crystal structure is due to the presence of the uncompensated positive charges. For example, the distances between the Cu's and the angle of the T3a−O−T3b bridge are greater than the experimental values (by ~0.3 Å and ~14°, respectively).

(62) It should be noted that this pH effect is independent of the buffer used; MES, potassium phosphate, and potassium phthalate buffers yield similar results.
(63) Sillen, L. G.; Martell, A. E. *Stability Constants of Metal-Ion Complexes*; The Chemical Society: London, 1974.
(64) Groves, J. T.; Chambers, J. R. R. *J. Am. Chem. Soc.* **1984**, *106*, 630−638.
(65) Groves, J. T.; Olson, J. R. *Inorg. Chem.* **1985**, *24*, 2715−2717.
(66) Nitta, K.; Kataoka, K.; Sakurai, T. *J. Inorg. Biochem.* **2002**, *91*, 125−131.
(67) Randall, D. W.; DeBeer-George, S.; Hedman, B.; Hodgson, K. O.; Fujisawa, K.; Solomon, E. I. *J. Am. Chem. Soc.* **2000**, *122*, 11620−11631.

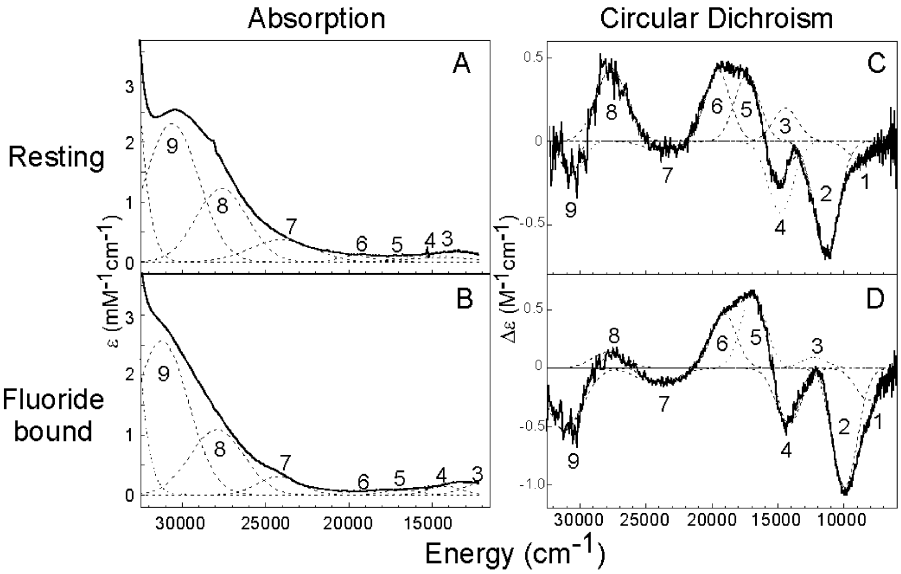

Figure 5. Room-temperature difference absorption spectra of resting (A) and fluoride-bound (B) T1Hg laccase at pD 7.5, and circular dichroism spectra of resting (C) and fluoride-bound (D) T1Hg laccase. The absorption spectrum of reduced T1Hg laccase has been subtracted from the original spectra in order to subtract the intense contribution from the protein absorbance. Resolved component Gaussian bands are shown in dotted lines, and their parameters are listed in Table 3.

Table 3. T3 Site: Absorption and CD Transition Energies (cm^{-1})

band assignment	T1HgLc resting	$\Delta\epsilon/\epsilon$	T1HgLc fluoride adduct	$\Delta\epsilon/\epsilon$
1 d−d	(−) 8 800	ND	(−) 8 200	ND
2 d−d	(−) 11 400	ND	(−) 9 900	ND
3 d−d	(+) 14 400	0.0027	(+) 12 300	ND
4 d−d	(−) 14 800	−0.0041	(−) 14 200	−0.00327
5 d−d	(+) 17 400	0.0070	(+) 16 900	0.00709
6 d−d	(+) 19 600	0.0039	(+) 19 100	0.00709
7 His π−T3 Cu	(−) 24 000	−0.00013	(−) 24 200	−0.000436
8 OH−T3 Cu	(+) 27 600	0.00036	(+) 27 900	0.000127
9 OH−T3 Cu	(−) 30 600	−0.000089	(−) 31 200	−0.000207

The ground-state descriptions of the T2 and T3 sites are given in Tables 5 and 6, respectively. Both the percent composition in the respective unoccupied orbital and the spin density (in parentheses) are presented (B38HFP86/VTZ*+6-31G* level). These values directly correlate to the bonding interactions between the metal and its ligands. In particular, the spin-unrestricted broken symmetry wave functions allow separate descriptions of the magnetic orbitals involved in exchange coupling. Figure 6 shows the contours of the unoccupied molecular orbitals (MOs), describing the bonding interactions at the T2 and T3 sites. Consistent with early ligand field[18] calculations, the three-coordinate T2 site (Figure 6a) has a $d_{x^2-y^2}$ ground state and a square-planar environment with an open coordination position oriented toward the center of the cluster. The T3 Cu centers (Figure 6b,c) have d_{z^2} ground states and are best described as trigonal bipyramidal sites with open equatorial positions also oriented toward the center of the cluster. Finally, the isotropic constant J's ($\hat{H} = -2JS_1 \cdot S_2$) are similar between isolated T3 and T2T3, as shown in Table 7. Therefore, the T2 is electronically and magnetically isolated from the T3 site in T2T3.

The dominant contribution in the electronic structure of the T2 site is the σ-bond interaction between Cu $d_{x^2-y^2}$ and O p_x of OH^- (Figure 6a). The interactions between Cu $d_{x^2-y^2}$ and the histidine ligands are also of σ type, but weaker. The ground-state description for the T2 site is in reasonable agreement with the experiment (Table 5); however, the description of the Cu−O bond is too covalent.[68] This discrepancy can be resolved by including the protein dielectric media using a PCM model ($\epsilon = 5.0$), and modeling the hydrogen bonding in the vicinity of the OH ligand. Comparing T2, T2(PCM), T2+HB, and T2+HB(PCM) in Table 5, the dielectric media and hydrogen bonding increase the Cu character of the ground state by 3.4% and 2.8%, respectively. The total Cu character for the T2+HB-(PCM) model is in good agreement with the experimental data.

The description of the T2 Cu^{II}−OH bond in the T2T3 calculation is more covalent than in the T2 model (Table 5). This was investigated by calculating the effects on the T2 model of two point charges at the location of T3 Cu's and with their Mulliken charges of $\sim +0.5$. The T2 Cu character is reduced by ~7% (Table S3, Supporting Information), and therefore, the high Cu−O covalency appears to originate from the electrostatic repulsion associated with the unshielded charges.

The binding energy obtained when the T2 and T3 sites were combined to form the T2T3 cluster was +183 kcal/mol, reflecting the large repulsive energy between the positive charges of the Cu centers. This repulsive energy is lowered by 129 kcal/mol (to +54 kcal/mol) when a PCM ($\epsilon = 5$) is introduced. Moreover, the positive charges are neutralized by the surrounding protein pocket. The crystal structures of several multicopper oxidases show the presence of negatively charged residues in the vicinity of the cluster (at least four Asp/Glu residues within 12 Å). The Coulombic interactions between the cluster and these carboxylic residues were modeled, and the electrostatic stabilization energy is estimated to be −80 kcal/mol at $\epsilon = 5.0$.[69] Overall, the negative charges in the vicinity and the protein dielectric strongly stabilize the highly charged trinuclear Cu^{II} site.

(68) Experimental results are best matched by B38HFP86/VTZ*+6-31G*. Other methods, such as B3LYP, gave much more covalent descriptions of the Cu−O bond in T2, with Cu characters <50%.

(69) Charges on the atoms in the T2T3 site were taken from either Mulliken population analysis or natural population analysis (NPA) in the DFT calculations, and the four Asp/Glu residues were treated as point −1e charges ($\epsilon = 5$).

Table 4. Selected Geometry Parameters of the Optimized Structures of Trinuclear Cu Cluster and Its Fluoride-Bound Form (Distances are Given in Angstroms and Angles in Degrees)[a]

	r(CuCu)[b]	r(CuO$_{T2}$)	r(CuO$_b$)[c]	θ(CuO$_b$Cu)	r(Cu–F)[d]	θ(CuFCu)[e]
exptl (1aoz)	*3.66/3.78/3.69*	*2.02*	*2.06/1.99*	*131.0*		
T2		1.90				
T2+HB[f]		1.90				
T3	−/−/3.72		2.01/1.97	138.4		
T2T3	4.07/4.19/3.84	1.89	2.03/2.00	144.5		
T2T3+HB[f]	4.04/4.20/3.85	1.90	2.04/2.00	144.8		
T2+F$^-$		1.92			1.92/−/−	
T3+F$^-$	−/−/3.18		1.98/1.95	107.9	−/2.03/2.05	−/−/102.5
T2T3+F$^-$	3.80/3.80/3.33	1.89	2.00/1.95	114.9	2.07/2.12/2.19	130.2/126.4/101.1

[a] Each structure was optimized at the uB3LYP/LanL2Dz level of theory. T2 and T3 refer to the isolated Cu sites of the trinuclear cluster, respectively. T2T3 refers to the whole trinuclear cluster. T2+F$^-$, T3+F$^-$, and T2T3+F$^-$ refer to the F$^-$-bound forms. [b] T2−T3a, T2−T3b, and T3a−T3b distances, respectively. [c] T3a−O and T3b−O (O being the bridging O-ligand between the T3 Cu's) distances, respectively. [d] T2−F, T3a−F, and T3b−F distances, repectively. [e] T2−F−T3a, T2−F−T3b, and T3a−F−T3b angles, respectively. [f] T2+HB and T2T3+HB refer to structures with two H_2O molecules near the T2 site, mimicking the ambient hydrogen bond network.

Table 5. Ground-State Descriptions of the T2 Cu Site from the DFT Calculations on the Resting Oxidized Trinuclear Cu Cluster (T2T3) and the Isolated T2 Site (T2) Models[a]

	Cu(T2)	OH	His[b]	F$^-$
exptl	*70%*	*≥13%*	*15%*	
T2	63.1 (0.58)	27.6 (0.34)	9.3 (0.08)	
T2 (PCM)	66.5 (0.62)	24.2 (0.30)	9.3 (0.08)	
T2+HB	65.9 (0.62)	23.9 (0.30)	9.9 (0.08)	
T2+HB (PCM)	69.3 (0.65)	20.6 (0.26)	10.0 (0.09)	
T2T3[c]	56.7 (0.53)	33.0 (0.41)	7.9 (0.05)	
T2T3+HB[c]	58.5 (0.55)	30.2 (0.39)	8.1 (0.07)	
exptl	*70%*	*ND*	*14%*	*7%*
T2+F$^-$	69.1 (0.68)	9.3 (0.12)	15.9 (0.12)	5.7 (0.08)
T2+F$^-$ (PCM)	61.1 (0.68)	8.5 (0.12)	26.3 (0.13)	4.1 (0.07)
T2T3+F$^-$ [c]	67.0 (0.66)	15.2 (0.20)	13.1 (0.11)	2.0[d] (0.03)

[a] Compositions (%) in the βLUMO and the spin densities (in parentheses) are presented. See Table 4 for descriptions of the models. [b] The spin densities for the two histidine ligands have been added. [c] PCM calculations on T2T3 models were not possible due to their large sizes. [d] F$^-$ character in the T2-based αLUMO+1 orbital.

2. Electronic Structure of the Fluoride Adduct. 2.1. Spectroscopic Characterization of the T2 Site in the Fluoride Adduct.

2.1.1. Multifrequency EPR. The EPR spectra of the T2 site in the fluoride adduct of T1Hg laccase have been collected at different microwave frequencies. The X-band EPR spectrum at 77 K (Figure 1D) shows well-resolved doublets in the parallel region that originate from a single fluoride ($I = {}^1/_2$) binding equatorially with a superhyperfine coupling of ∼63 × 10^{-4} cm^{-1}, as previously reported.[17] In the Q-band EPR spectrum at 34 GHz (Figure 1E), the parallel region is clearly separated from the perpendicular region, and the fluorine superhyperfine splitting is resolved at each one of the four M_S transitions derived from the Cu ($I = {}^3/_2$) hyperfine splitting. The structure observed in the perpendicular region of the X- and Q-band spectra is due to both fluoride and nitrogen superhyperfine couplings. Finally, in the 285 GHz EPR spectrum (Figure 1F), the rhombicity in the perpendicular region is resolved and a large fluorine superhyperfine splitting (∼160 × 10^{-4} cm^{-1}) occurs along the smallest g value (g_x). The simultaneous fit of these multifrequency EPR spectra yields the spin Hamiltonian parameters listed in Table 1, and the simulated spectra are shown in Figure 1 (dotted lines).

Relative to the resting form, the g values increased in the fluoride adduct (Table 1), and their rhombicity decreased slightly ($g_y - g_x = 0.011$). The increase in g values mostly reflects a decrease in the LF transition energies, as observed by MCD (section 2.1.5 and Table 2). From ligand field theory,[45] the differences of g_x and g_y from 2.00 are inversely proportional to the $d_{yz} \rightarrow$ and $d_{xz} \rightarrow d_{x^2-y^2}$ LF transition energies, respectively. Therefore, the decreased rhombicity reflects changes in the energy splitting between these two transitions (i.e., 2200 cm^{-1} in resting to 1400 cm^{-1} in fluoride adduct, Table 2).

The Cu hyperfine coupling values did not change significantly in the fluoride adduct. Following an analysis of the spin Hamiltonian parameters given for the resting form (vide supra), and using the g and A values for the fluoride adduct (Table 1), the ground state of the T2 in the fluoride adduct is also estimated to have ∼70% Cu character.

The largest fluorine superhyperfine tensor component must be aligned along the Cu−F bond; therefore, A_x^F from Figure 1F corresponds to $A_\parallel^F$ (in the ligand coordinate system). The superhyperfine splitting along the g_y direction is not large enough to be resolved, but EPR simulations indicate that this has a value similar to A_z^F, which corresponds to $A_\perp^F$ (in the ligand coordinate system). The superhyperfine couplings from fluoride are given by

$$A_\parallel^F = \beta^2[n^2A_{iso} + (1 - n^2)A_{aniso}] \quad (4a)$$

$$A_\perp^F = \beta^2[n^2A_{iso} - {}^1/_2(1 - n^2)A_{aniso}] \quad (4b)$$

where β^2 is the electron spin density at the fluoride, n^2 is the s character of the fluoride orbital, and A_{iso} and A_{aniso} for ^{19}F are 17 630 × 10^{-4} and 1010 × 10^{-4} cm^{-1}, respectively.[51,52] From the experimental $A_\parallel^F = 160 \times 10^{-4}$ cm^{-1} and $A_\perp^F = 63 \times 10^{-4}$ cm^{-1}, ∼7% spin density is estimated for the fluoride. Fluorine couplings in CuF$^+$(aq) have been measured: $A_{iso}^F = 333 \times 10^{-4}$ cm^{-1} and $A_{aniso}^F = 273 \times 10^{-4}$ cm^{-1}.[70] From these values, 20% spin density is estimated for the equatorial fluoride ligand. Therefore, the spin density at the fluoride in the T1Hg laccase adduct is small in comparison, indicating that the T2 Cu−F bond is significantly weaker than a normal Cu^{II}−F bond. The relatively weak T2 Cu^{II}−F bond is quite interesting, considering that fluoride binds to the cluster with >10^5 higher affinity than to aqueous copper complexes.[21,71]

The fact that the largest superhyperfine tensor component is along the smallest g value direction (g_x) implies that the direction of fluoride binding corresponds to a stronger ligand field (if $g_x < g_y$, then $\Delta E_{yz} > \Delta E_{xz}$, which means that the d_{xz} orbital is

(70) Eisenstadt, M.; Friedman, H. L. *J. Chem. Phys.* **1968**, *48*, 4445−4458.
(71) Winkler, M. E.; Spira, D. J.; LuBien, C. D.; Thamann, T. J.; Solomon, E. I. *Biochem. Biophys. Res. Commun.* **1982**, *107*, 727−734.

Table 6. Broken-Symmetry Ground-State Descriptions of the T3 Cu's on the Resting Oxidized Trinuclear Cu Cluster (T2T3) and the Isolated T3 Site (T3) Models[a]

	T3a	T3b	OH	$His_{ax,T3a}$[b]	$His_{eq,T3a}$[b]	$His_{ax,T3b}$[b]	$His_{eq,T3b}$[b]	F^-
T3	0.9/78.6	79.3/0.9	3.6/3.6	0.0/7.0	0.3/9.7	7.0/0.0	9.0/0.2	
	(0.77)	(−0.78)	(0.00)	(0.07)	(0.10)	(−0.07)	(−0.09)	
T2T3	0.8/79.5	78.2/1.9	3.4/3.6	0.0/6.8	0.3/10.2	6.5/0.2	9.9/0.2	
	(0.77)	(−0.77)	(0.00)	(0.07)	(0.10)	(−0.07)	(−0.10)	
T2T3+HB	0.9/79.4	78.3/2.0	3.5/3.4	0.0/6.2	0.3/10.3	6.5/0.2	9.8/0.2	
	(0.76)	(−0.77)	(0.00)	(0.08)	(0.10)	(−0.07)	(−0.10)	
$T3+F^-$	79.6/0.6	0.6/79.2	4.9/4.7	5.4/0.1	5.0/0.4	0.2/5.6	0.3/5.1	3.4/3.6
	(−0.78)	(0.78)	(0.00)	(−0.06)	(−0.04)	(0.06)	(0.04)	(0.00)
$T2T3+F^-$	0.5/79.2	79.3/0.6	5.2/5.0	0.1/5.4	0.4/6.2	5.4/0.1	6.6/0.3	1.6/1.6[c]
	(0.78)	(−0.78)	(0.00)	(0.06)	(0.06)	(−0.06)	(−0.06)	(0.03)

[a] Compositions in the αLUMO and βLUMO are presented in order. Spin densities are presented in parentheses. See Table 4 for descriptions of the models. PCM calculations on these models were not possible due to their large size. [b] Subscript "ax" refers to the axial histidines along the local *z*-axis and "eq" refers to the equatorial histidines in the local *x,y* plane of each Cu site. The "eq" values are the sum of the two equatorial histidine ligands at each Cu site. [c] F^- characters in the T3a/T3b-based αLUMO/βLUMO orbitals.

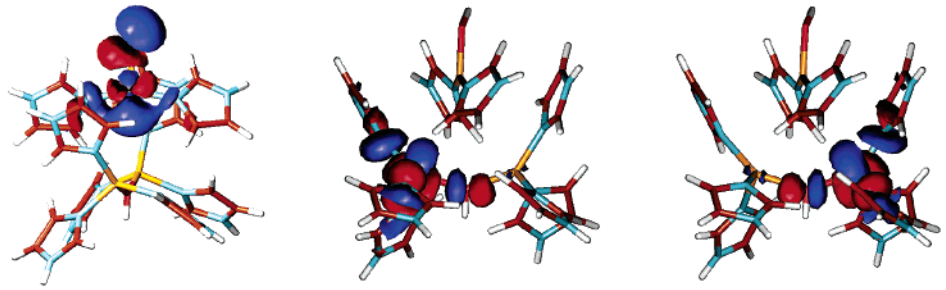

(a) Type 2 Copper: "$d_{x^2-y^2}$"; beta, unoccupied **(b) Type 3a Copper: "d_{z^2}"; alpha, unoccupied** **(c) Type 3b Copper: "d_{z^2}"; beta, unoccupied**

Figure 6. Surface plots of unoccupied molecular orbitals obtained from unrestricted DFT calculations.

Table 7. Isotropic Exchange Constant *J* of the Models[a]

	J (cm^{-1})		J (cm^{-1})
exptl	*< −200*	T3+F^- (w/o OH^-)[b]	−78.9
T3	−244.6	T2T3+F^- (w/o OH^-)[b]	−19.1
T2T3	−230.3	T2T3+{OH^-}[c]	−265.4
$T3+F^-$	−212.6	T2T3+{H_2O}[c]	−126.3
$T2T3+F^-$	−258.4		

[a] *J* values were determined by taking the energy difference between the high-spin state (quartet for T2T3, triplet for T3) and the broken symmetry state. [b] Single-point calculations of the T3/*T*2T3 models with F^- but without the bridging OH^- between T3 Cu's. [c] T2T3 models with OH^-/H_2O at the center of the cluster.

more destabilized than the d_{yz} orbital due to a stronger ligand field along the *x* direction). The relative ligand field strength affecting the d_{xz} and d_{yz} orbitals is determined by the strength of the hydroxide ligand relative to the two histidines (^{2}H ENDOR results indicate that the hydroxide is still bound in the presence of fluoride, section 1.1.4). Although histidines are reasonable donor ligands, the charge donation from the anionic hydroxide is quite significant (section 1.3). Therefore, fluoride binds to the T2 site along the open equatorial coordination position that is trans to the hydroxide ligand and along the *x* direction.

2.1.2. Nitrogen ENDOR. The Davies ENDOR spectrum of the fluoride adduct of T1Hg laccase at pH 7.5 (Figure 2D) is very similar to that of the resting form (Figure 2A). The proton resonances dominate the $\pi = 400$ ns and $\pi/2 = 200$ ns pulse spectrum (dotted line in Figure 2D), while the nitrogen resonances are enhanced in the $\pi = 60$ ns and $\pi/2 = 30$ ns pulse spectrum (solid line in Figure 2D) and correspond to $A^N/2 = 20.7$ MHz. The nitrogen coupling has decreased with respect to the resting site, and from the $A^N = 41.4$ MHz (13.8×10^{-4} cm^{-1}) value, a total spin density of ~14% is calculated for the nitrogens. Therefore, the binding of fluoride has slightly decreased the covalency of the T2 Cu−histidine interactions.

2.1.3. Nitrogen ESEEM. The three-pulse ESEEM spectrum of the T1Hg laccase fluoride adduct (Figure 2E) is very similar to that of the resting form (Figure 2B). The presence of a combination peak at around 2.5 MHz denotes that the Cu center still has more than one coordinated histidine. Small intensity differences are observed in the double-quantum peak at 4 MHz, reflecting small changes in the coupling of the remote nitrogens.

2.1.4. Deuterium ENDOR. The Mims ENDOR spectrum of the T1Hg laccase fluoride adduct (Figure 2F) is very similar to that of the resting form (Figure 2C), indicating that the strongly coupled ^{2}H are still present in the fluoride adduct. This is confirmed by the ^{1}H two-pulse ESEEM spectrum (Figure S2, Supporting Information), which shows a peak shift from the $2\nu_H$ sum combination peak, similar to that observed in the resting form. These results indicate that the hydroxide ligand (vide supra) is still bound to the Cu center in the fluoride adduct.

In summary, cw EPR results indicate that one fluoride binds to the T2 Cu along its open equatorial coordination position, forming a relatively weak Cu−F bond, even though it binds with high affinity. Also, pulsed EPR results show that the two histidines and the hydroxide ligand are still bound in the fluoride adduct; therefore, the site becomes four-coordinate. It is interesting to note that although a fourth ligand has coordinated to the Cu site, the Cu character of the site remains unchanged, while the nitrogen character shows only a modest decrease.

2.1.5. MCD. The MCD spectrum of the T1Hg laccase fluoride adduct (Figure 3B) can be resolved into eight Gaussian bands, as listed in Table 2. The CT transitions show decreased

intensity and shift to higher energy, while the ligand field transitions (bands 1−4) show decreased intensity and their energies decrease by moderate amounts (200−600 cm^{-1}). The decreased intensity has been associated with fluoride perturbing the CT states, which is the dominant source of intensity mixing for the d → d transitions.[17] EPR results indicate that the T2 Cu site has become four-coordinate upon fluoride binding. An increase in coordination number destabilizes the d manifold; therefore, the CT transition energies increase. However, while CT transition energies normally increase by ∼6000 cm^{-1} with an increase in coordination number,[59] the CT transition energies in the T1Hg fluoride adduct increase only by ∼1500−3000 cm^{-1} (Table 2). Overall, the magnitudes of the spectroscopic changes observed are not as large as expected for a three to four coordination number change, indicating that the fluoride ligand−T2 Cu bond is weak.

2.1.6. pH Effects on the T2 Site. The spectroscopic features of the T2 site in the T1Hg laccase fluoride adduct were investigated at pD 4.7 and pD 7.5. The LF region of the MCD spectrum of the fluoride adduct shows a pH effect similar to that observed in the resting form (i.e., a positive band at ∼7800 cm^{-1} grows in at low pH, Figure S7A, Supporting Information), while the multifrequency EPR spectra show no changes with pH (Figure S7, Supporting Information). Similarly, the CD spectra of the fluoride adducts show no changes, indicating that the T3 site is not perturbed with change in pH (Figure S8, Supporting Information). The deuterium ESEEM spectra (Figure S7E) show a pH effect similar to that observed in the resting form (i.e., deeper modulation at high pH), yet smaller in magnitude. These results indicate that the pH effect observed in the resting T2 Cu site is preserved in the fluoride adduct, consistent with the observations that the hydroxide ligand has not been displaced by fluoride (vide supra) and that fluoride binds at the inner T2 position of the cluster (vide infra).

2.2. Spectroscopic Characterization of the T3 Site in the Fluoride Adduct. The absorption and CD spectra of the T1Hg laccase fluoride adduct are shown in panels B and D of Figure 5, respectively. Simultaneous Gaussian fitting of the absorption and CD spectra requires the presence of nine bands with the parameters listed in Table 3. All ligand field transitions (bands 1−6) shift to lower energy upon fluoride binding, indicating that the ligand is interacting with *both* T3 Cu centers. Since EPR and MCD studies have shown that fluoride also binds to the T2 site, this ligand must bridge and likely binds within the trinuclear cluster at the open coordination positions of the three Cu centers. This is consistent with the geometry optimizations obtained by DFT (section 2.3).

The CT transitions (bands 7−9) show a modest shift to higher energy (Table 3) and a redistribution of intensity. In particular, the intensity of band 8 decreases, while that of band 9 increases (Figure 5D); the changes are most evident in the overall shape of the broad absorption band at ∼30 300 cm^{-1} (Figure 5B). Bands 8 and 9 correspond to the μ-OH → Cu^{2+} CT transitions; thus, the observed changes demonstrate that fluoride binding to the T3 site perturbs the nature of the hydroxide bridge. Overall, the changes observed upon fluoride binding are quite moderate for four to five coordination changes, suggesting that each T3 Cu−fluoride interaction is also weak.

2.3. DFT Calculations on the Fluoride Adduct. The DFT calculations on the fluoride (F^-) adduct of the resting oxidized (T2T3) trinuclear cluster site have been performed to correlate to spectra and gain further insight into the geometric and electronic structure of this complex. This also serves as an experimentally calibrated reference for evaluating the energetics of exogenous ligand binding (section 3). The geometrical parameters obtained from optimizations of the F^- adduct (T2T3+F^-) along with F^--bound forms of the isolated T2 and T3 sites are listed in Table 4. These calculations show that the anion preferably occupies the open coordination positions of the T2 and T3 sites in the center of the cluster. Comparison of the Cu−F distances in T2+F^-, T3+F^-, and T2T3+F^- shows that the Cu−F bonds are longer in the T2T3+F^- structure by ∼0.1 Å, suggesting that each Cu−F bond in the T2T3+F^- model is weakened by the presence of the additional Cu−F interactions. MO descriptions and spin densities also indicate weaker Cu−F bonds in the T2T3 cluster as the F^- character is reduced in the trinuclear environment (T2+F^- (5.7%) vs T2T3+F^- (2.0%) or T3+F^- (3.5%) vs T2T3+F^- (1.6%); Tables 5 and 6). This is consistent with the spectroscopic results.

The isotropic exchange constant J for the fluoride adduct (Table 7) demonstrates that F^- provides a poor superexchange pathway. The J's are not significantly changed after F^- binding to the T2T3 cluster (−230 vs −258 cm^{-1}, respectively). The contribution of the F^- bridge to J was tested by removing the OH^- bridge between T3 Cu's. The resultant J is small (−19 cm^{-1}), demonstrating that the T2 and T3 Cu's are still electronic and magnetically isolated in the T2T3+F^- model. Therefore, the interaction between the trinuclear cluster and the F^- ion is dominantly electrostatic in nature, with only a limited covalent contribution.

3. DFT Calculations on the Energetics of μ_3-Ligand Binding to the Trinuclear Cluster. The energy profiles of the binding of exogenous ligands F^-, H_2O, and OH^- at the center of the trinuclear cluster have been evaluated using DFT calculations as presented in Figure 7. For each process, the following sequence is considered: (1) desolvation of the exogenous ligand from aqueous solution ($\epsilon = 80$), (2) desolvation of the trinuclear site (T2T3) from the protein dielectric media ($\epsilon = 5.0$), (3) binding of the ligand to the T2T3 cluster in a vacuum, and (4) re-solvation of the ligand-bound T2T3 cluster.[72] In addition, the energies of the resting T2T3 (+4e) and ligand-bound forms (+3e) were adjusted by the electrostatic stabilization of the positively charged cluster by the four nearest carboxylic residues ("Asp/Glu effect" in Figure 7).[73]

A dominant contribution to the high stability of the F^--bound T2T3 complex (Figure 7A) is the binding energy of F^- to the T2/T3 cluster in a vacuum (−375 kcal/mol). The nature of this binding is largely electrostatic, as the Coulombic energy (using point charges from Mulliken or natural population analysis) is ∼ −300 kcal/mol. Opposing this is the net solvation energy of +306 kcal/mol (desolvation of F^- (+112 kcal/mol), desolvation of T2T3 (+455 kcal/mol), and re-solvation of T2T3+F^- (−261 kcal/mol)), which destabilizes the binding. With inclusion of the protein pocket stabilization effects (Asp/Glu effect), an overall energy of −42 kcal/mol is obtained. The F^- affinity

(72) The solvation energies were obtained with PCM calculations on models designed with NH_3 substituted for the histidine ligands.

(73) This electrostatic stabilization by the protein pocket is dependent on the total charge of the active site. With a dielectric constant of $\epsilon = 5.0$, a stabilization energy of ∼80 kcal/mol was obtained when the total charge of the active site is +4 (T2T3 or T2T3+H_2O), and ∼53 kcal/mol was obtained when the total charge is +3 (T2T3+F^- or T2T3+OH^-).

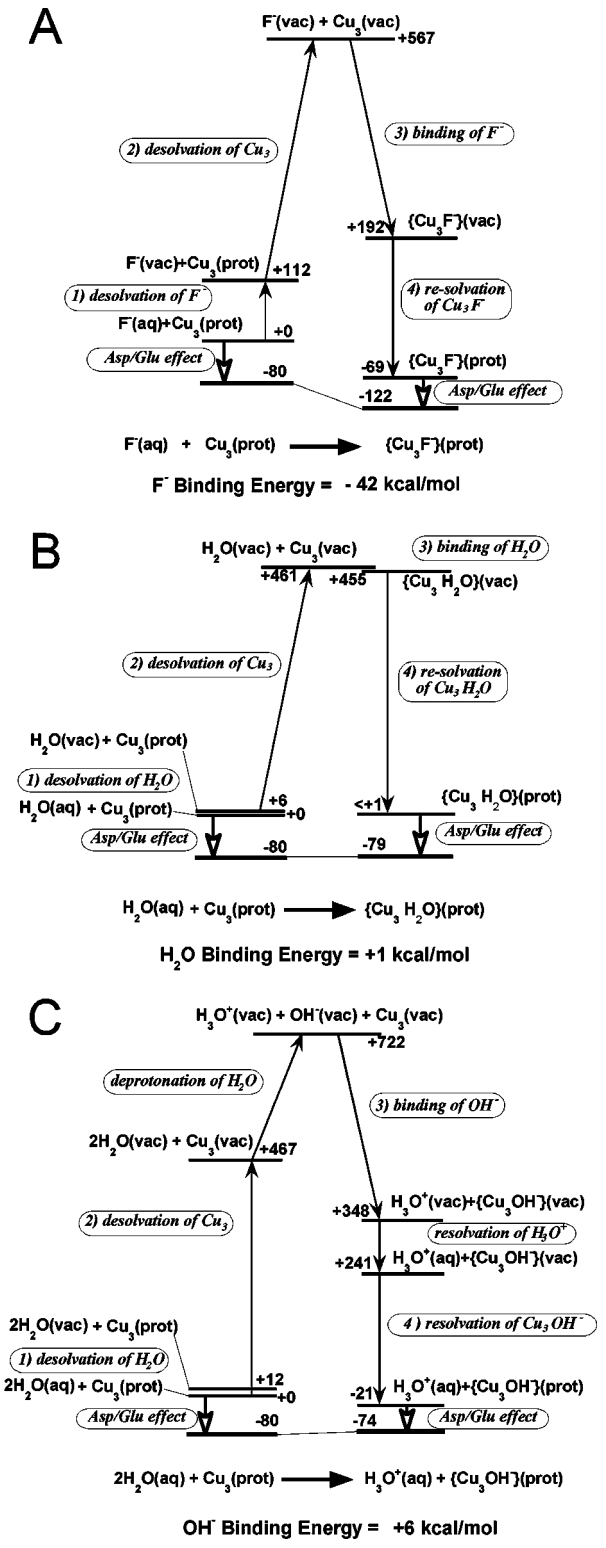

Figure 7. Energy profile of the binding process of F^- (A), H_2O (B), and OH^- (C) into the Cu^{II}_3 center (in kcal/mol). (aq) and (prot) refer to the aqueous ($\epsilon = 80$) and the protein ($\epsilon = 5$) dielectric media, respectively, (vac) refers to the non-dielectric environment, and "Asp/Glu effect" refers to the electrostatic stabilization by the four nearest carboxylic residues in the surrounding protein environment.[73]

(K_f) of the trinuclear cluster has been experimentally determined to be at least 10^5 that of a monomeric Cu^{II} complex in aqueous solutions (i.e., >7 kcal/mol more favorable). To evaluate this point, a set of DFT calculations were performed on the binding of F^- to a monomeric aqueous Cu^{II} model complex. This involved F^- substitution of a H_2O bound to a Cu^{II} complex with two NH_3 ligands and one OH^- ligand (i.e., resembling the T2 site) in an aqueous environment ($\epsilon = 80$). The overall energy for this process (−30 kcal/mol, Figure S9) was found to be 12 kcal/mol less favorable than for F^- binding to the T2T3 site (Figure 7A). If more complex−solvent interactions are considered, this difference would be larger as the overall binding energy would be less favorable due to a larger $Cu^{II}-H_2O$ dissociation energy term. Thus, the lower stabilization from F^- binding to an aqueous monomeric Cu^{II} complex is not as efficient in overcoming the desolvation energies involved, resulting in the relatively lower F^- affinity.

In contrast to the high affinity calculated for F^- binding to the T2T3 cluster, binding of H_2O is nearly isoenergetic (less than +1 kcal/mol; Figure 7B). The dominant terms in this process are mainly the desolvation of the T2T3 site and re-solvation of the H_2O-bound T2T3 cluster, although these are nearly equal in magnitude. The desolvation energy of the H_2O molecule (+6 kcal/mol) and the binding of H_2O with the T2T3 site (−6 kcal/mol) result in only a negligible contribution to this process. In contrast to F^-, where binding to T2T3 is very exothermic, the binding energy of the H_2O to the T2T3 cluster is essentially zero, as the stabilization of the H_2O−T2 Cu^{II} binding is counteracted by the steric destabilization of having a relatively bulky H_2O molecule inside the cluster (geometry optimization parameters are given in Table S4, Supporting Information). The total charge of the cluster does not change upon H_2O binding; thus, the electrostatic stabilization by the nearby carboxylic residues is the same for both the T2T3 and T2T3+H_2O sites.

However, H_2O can deprotonate and produce OH^- (Figure 7C), which can have an equally strong electrostatic attraction to the T2T3 cluster site as F^-. The optimized structure of an OH^--bound T2T3 cluster site has the anion in the center (Table S4, Supporting Information), similar to the optimized structure of T2T3+F^- (Table 4), and the OH^- binding energy in vaccum is −374 kcal/mol, essentially the same as the F^- binding energy in vacuum. However, the F^- and OH^- binding processes are different in that the former involves desolvation of F^- (+112 kcal/mol), whereas the latter involves a combination of desolvation of H_2O (+12 kcal/mol), deprotonation of H_2O (+255 kcal/mol), and re-solvation of H_3O^+ (−107 kcal/mol), which amounts to +160 kcal/mol. Therefore, the OH^- binding process is 48 kcal/mol less favorable than F^- binding, resulting in an overall energy of +6 kcal/mol. It is important to note that, since the resting trinuclear site has a charge of +4 and the OH^--bound form has a charge of +3, their relative stabilization by the negatively charged carboxyl residues in the vicinity of the cluster favors the unbound form by 27 kcal/mol, resulting in an endothermic process.

Discussion

A combination of spectroscopic and DFT studies has led to significant insight into the geometric and electronic structures of the resting trinuclear Cu cluster active site in laccase, which is prototypical of the known multicopper oxidases. In particular, spectroscopic studies have clarified the nature of the T2 Cu ligation; this site is three-coordinate with two histidine ligands and a hydroxide at all pH's. This is consistent with crystallographic results on several multicopper oxidases,[6−12] which

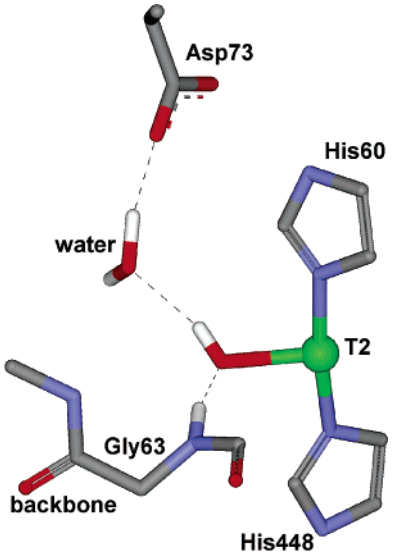

Figure 8. Hydrogen-bonding network around the T2 Cu water-derived ligand. Figure generated from the crystal structure of AO (PDB accession number 1AOZ).[6] Hydrogens were added in DS Viewer Pro 5.0 (Accelrys).

show a three-coordinate T2 site at different temperatures (100−277 K). The water-derived ligand at the T2 site is stabilized in the hydroxide form by the large inductive effect associated with the low coordination of the T2 Cu^{II} site, the high positive charge of the cluster, and the hydrogen-bonding network to the coordinated hydroxide. The crystal structures of AO[6] and the other multicopper oxidases[7−12] show that the backbone amide of Gly63 (Gly62 in *Rhus vernicifera* laccase)[66] is hydrogen-bonded to the hydroxide ligand at the T2 center (O−N distance = 3.1 Å), as shown in Figure 8. A second hydrogen bond connectivity of the T2 OH ligand appears to involve an Asp residue (Asp73 in AO, Asp72 in *Rhus vernicifera* laccase),[66] as suggested by the pH dependence of the T2 Cu MCD spectrum ($pK_a = 5.5 \pm 0.8$).[74,75] The carboxylic moiety of Asp73 is hydrogen-bonded to a water molecule, which in turn is hydrogen-bonded to the T2 OH ligand (Figure 8). The fact that this hydrogen bond network around the T2 hydroxide ligand is highly conserved among all multicopper oxidases suggests that this arrangement may be implicated in the stability and reactivity of the site.

The geometric and electronic structure descriptions obtained from DFT calculations correlate well with the spectroscopy and crystallography. The T2 Cu is a three-coordinate site with a planar geometry, a $d_{x^2-y^2}$ ground state, and an open coordination position oriented toward the center of the cluster. The T3 Cu centers are four-coordinate but with d_{z^2} ground states and an energy level splitting indicating a trigonal bipyramidal geometry with each T3 Cu having an open equatorial position also oriented into the center of the cluster. It is important to emphasize that the resting trinuclear cluster is thus highly coordinatively unsaturated, yet with unusual ligand binding properties. A second important property of the resting oxidized trinuclear Cu cluster is that the positive charge of three Cu^{II} centers is not compensated by the Cu ligands. With an OH^- bridge at the T3 site and a terminal OH^- ligand at the T2 site, the total charge of the cluster is +4. This positive charge is neutralized and the repulsive energy is stabilized by the protein matrix in the vicinity of the site. DFT calculations (with PCM and Coulombic models) have shown that the negative protein pocket (four conserved Asp/Glu residues within 12 Å) and the dielectric of the protein play important roles in the electrostatic stability and integrity of the highly charged trinuclear Cu^{II} cluster.

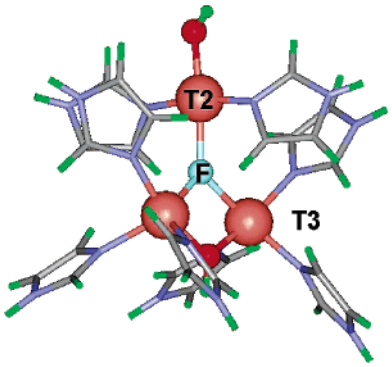

Figure 9. Geometry-optimized structure of the F^--bound trinuclear Cu cluster. Structural parameters are given in Table 4.

A characteristic property of the resting trinuclear cluster of the multicopper oxidases is its high affinity for fluoride, which is at least 10^5 larger than that of aqueous Cu^{II} (i.e., >7 kcal/mol more favorable). DFT calculations indicate that F^- binding to a monomeric Cu^{II} complex is less favorable than F^- binding to the trinuclear cluster by 12 kcal/mol. However, spectroscopy and DFT calculations indicate that the resulting Cu−F bonds in the F^- adduct of the cluster are ~3 times weaker than a mononuclear Cu−F covalent interaction (as assessed by EPR). A simple electrostatic model predicts a F^- binding energy to the trinuclear cluster that is comparable in magnitude to the DFT-derived value, indicating that the nature of this binding is largely electrostatic. Thus, the high affinity of the trinuclear cluster for fluoride comes dominantly from the electrostatic interaction of the negative charge at the center of the positive cluster and the decrease in electrostatic repulsion among the Cu^{II} ions. This electrostatic stabilization overcomes the large desolvation energy required to bind the F^- to the center of the cluster (Figure 9).

Given that the electrostatic repulsion between the three Cu centers provides the large driving force for anion binding, it is important to consider why water does not deprotonate and bind as hydroxide to the center of the resting trinuclear cluster. DFT results indicate that the energy loss from deprotonating a water molecule to generate hydroxide can be compensated by the stabilization energy from OH^- binding in a μ_3 fashion to the center of the cluster, similar to the fluoride (Figure 9); however, the electrostatic stabilization by the carboxylic residues in the vicinity ("Asp/Glu effect" in Figure 7) is larger for the resting site (total charge of +4) than for the hydroxide-bound cluster (+3) by 27 kcal/mol, rendering this process unfavorable and resulting in open coordination positions on the T2 and T3 coppers inside the cluster. Thus, the differential electrostatic stabilization provided by the protein matrix contributes to the coordination unsaturation of the trinuclear Cu cluster in aqueous solution.

The coordination unsaturation of the trinuclear cluster is likely of functional significance. Having open coordination positions

(74) It should be noted that mutations at this conserved aspartate in the multicopper oxidase Fet3p have demonstrated that this residue is responsible for the pH effect observed by MCD.[75]

(75) Quintanar, L.; Stoj, C.; Wang, T.-P.; Kosman, D. J.; Solomon, E. I. *Biochemistry* **2005**, *44*, 6081−6091.

facilitates O_2 binding within the cluster, while its reduction to negatively charged oxo/hydroxo species (as in the native intermediate)[76] results in bridged structures with total charges of $<+4$. The electrostatic environment of the protein pocket destabilizes these bridged structures, facilitating water release and keeping the site from product inhibition. It also prevents solvent water coordination as hydroxide to the resting cluster, which would stabilize the charged cluster, lower the redox potential, and thus tune the site out of the effective range for reduction of O_2 to H_2O.

In summary, spectroscopic and electronic structure studies have elucidated the nature of the T2 Cu ligation and provided a detailed geometric and electronic structure description of the trinuclear Cu cluster of the multicopper oxidases, complementing crystallographic results. This description emphasizes the coordination unsaturated nature of the trinuclear Cu site. An important conclusion from this study is that the anionic charge in the vicinity of the cluster appears to stabilize its high positive charge and tune its coordination unsaturation and redox properties, contributing to the O_2 reactivity of the trinuclear Cu cluster.

Acknowledgment. This research was supported by NIH Grants DK31450 (to E.I.S.) and GM48242 (to R.D.B.), by the European Commission ("Transnational Access—Specific Support Action" Program, Contract no. RITA-CT-2003-505474 and INTAS project 03-51-3945), and by the Grenoble High Magnetic Field Laboratory, CNRS, France. The authors thank Dr. Anne-Laure Barra (Grenoble) for assistance in running the HF-EPR facility and collecting HF EPR spectra.

Supporting Information Available: Simulations of the nitrogen ESEEM spectra of resting T1Hg laccase; absorption spectra of T1Hg and T2-depleted laccase; multifrequency EPR, Davies ENDOR, nitrogen ESEEM, absorption, and CD spectra of resting T1Hg laccase at pH 7.5 and 4.7; MCD, multifrequency EPR, deuterium ESEEM, and CD spectra of the T1Hg laccase fluoride adducts at pH 7.5 and 4.7; table of ligand field and charge-transfer transitions at the T2 Cu, as predicted by TD-DFT calculations; comparison of ground-state descriptions of the T2 Cu with OH^- and H_2O; energy profile for the binding process of F^- to a monomeric Cu^{II} complex in aqueous solution; table of spin densities of the T2 Cu as a function of point charges at the T3 Cu sites, from DFT calculations; geometry optimization parameters of OH^- and H_2O bound to the trinuclear cluster at the μ_3-positions; and complete ref 32. This material is available free of charge via the Internet at http://pubs.acs.org.

JA0421405

(76) (a) Lee, S. K.; George, S. D.; Antholine, W. E.; Hedman, B.; Hodgson, K. O.; Solomon, E. I. *J. Am. Chem. Soc.* **2002**, *124*, 6180−6193. (b) Yoon, J.; Mirica, L. M.; Stack, T. D. P.; Solomon, E. I. *J. Am. Chem. Soc.* **2005**, in press.